Scaled frequency-dependent transport in the mesoscopically phase-separated colossal magnetoresistive manganite $La_{0.625-y}Pr_yCa_{0.375}MnO_3$

S. Chaudhuri and R. C. Budhani*
Condensed Matter-Low Dimensional Systems Laboratory, Department of Physics, Indian Institute of Technology Kanpur, Kanpur-208016, India

Jiaqing He and Yimei Zhu
Department of Nanoscience, Brookhaven National Laboratory, Upton, New York 11973, USA
(Received 16 March 2007; revised manuscript received 4 June 2007; published 3 October 2007)

We address the issue of massive phase separation (PS) in the manganite family of doped Mott insulators through ac conductivity measurements on $La_{0.625-y}Pr_yCa_{0.375}MnO_3$ ($0.375 \leqslant y \leqslant 0.275$), and establish the applicability of the scaling theory of percolation in the critical regime of the PS. Measurements of dc resistivity, magnetization $[M(T)]$, and electron diffraction show incomplete growth of a ferromagnetic (FM) metallic component on cooling the high temperature charge-ordered (CO) phase well below the CO temperature. The impedance $|Z(T,f)|$ measured over a frequency (f) range of 10 Hz–10 MHz in the critical regime follows a universal scaling of the form $\approx R(T,0)g(f\xi^{2+\theta})$, with $\theta \approx 0.86$ and the normalized correlation length varying from 1 to 4, suggesting anomalous diffusion of holes in percolating FM clusters.

DOI: 10.1103/PhysRevB.76.132402 PACS number(s): 75.47.Lx, 64.60.Ak, 64.75.+g

The importance of phase separation (PS) in understanding the physics of manganite is vital.[1,2] Systems with strong electron correlations, like manganites, tend to be intrinsically phase segregated into regions with different electron densities. This coexistence of energetically near degenerate phases differing markedly in their properties makes manganites very susceptible to external perturbations such as electric, magnetic, and photon fields and pressure, thereby giving rise to the observed colossal responses.[3–6] One interesting doped manganite in which the phase separation has been imaged with a variety of techniques is $La_{0.625-y}Pr_yCa_{0.375}MnO_3$ (LPCMO). The end members of this pentanary compound, $La_{1-x}Ca_xMnO_3$ and $Pr_{1-x}Ca_xMnO_3$, are a ferromagnetic metal (FM) and a charge-ordered (CO) insulator, respectively, for the same doping level of $0.3 \leqslant x \leqslant 0.5$.[3,4] Thus, in LPCMO, even for a fixed doping (x), a transition from the FM to CO phase can be achieved by tuning the La/Pr ratio. X-ray diffraction[7] and optical studies[8] on LPCMO single crystals indicate that above the metal-insulator (MI) transition temperature T_{MI}, there also exists a charge-disordered (CD) insulating phase apart from the CO phase. Kiryukhin *et al.*[7] further proposed that the percolationlike MI transition seen in LPCMO is via the growth of the FM domains at the expense of the CD phase below the charge-ordering temperature (T_{CO}). Magneto-optical images of crystals of LPCMO ($y=0.3$), a related compound, revealed inhomogeneous magnetization and current distribution over a length scale of several micrometers due to phase separation.[9] Submicrometric phase separation in $La_{0.33}Pr_{0.34}Ca_{0.33}MnO_3$ thin films has also been seen with scanning probe microscopy (SPM) techniques.[10] Using electron diffraction and dark-field imaging, Uehara *et al.*[11] obtained phase separation of CO and FM domains over a scale of ≈ 0.5 μm at low temperatures. Thus, the PS as observed by most of these real space imaging techniques is over a micrometer length scale.[12] At such a length, the FM and CO clusters are large enough to treat electron transport through the system classically. Here, we apply the scaling theory of percolation to ac conductivity in a manganite which shows phase separation below a critical temperature T_{MI}. While this problem has been addressed theoretically by Mayr *et al.*[13] in the framework of a random resistor model, scaling analysis of the frequency-dependent conductivity which allows determination of the percolation correlation length ξ has been lacking, although a scaling between dc conductivity and magnetization has been shown for the system $Pr_{0.63}Ca_{0.37}MnO_3$.[14] In a classical metal-dielectric percolating system, the correlation length ξ diverges as $\xi \sim (p-p_c)^{\nu}$ as the metal concentration (p) approaches the percolation threshold (p_c). For $p > p_c$, the dc conductivity σ_{dc} scales as $(p-p_c)^{\mu} \sim \xi^{\mu/\nu}$ and the probability of belonging to the infinite conducting cluster is $P_{\infty} \sim (p-p_c)^{\beta}$, where μ, ν, and β are the critical exponents.[15] It has been pointed out that on a length scale (L) $b \ll L \ll \xi$ (where b is the microscopic lattice distance), the geometry of percolating clusters is self-similar and, on such a scale, all physical measurements are expected to reflect self-similarity and, therefore, the bulk properties should be independent of ξ.[16] One can then estimate the relative phase fraction (PF) of the coexisting phases from the value of ξ. Although the PF in certain manganites has been inferred from the SPM measurements, the surface sensitive nature of these techniques may not allow correct determination of the PF. In this Brief Report, we first establish phase separation in epitaxial films of $La_{0.625-y}Pr_yCa_{0.375}MnO_3$ indirectly through quantitative measurement of magnetization, and then present direct imaging of the FM and CO domains with Lorentz and dark-field electron microscopies, respectively. The ground state of this system is a metal with nearly equal FM and CO phase fractions. The FM component (p) diminishes with the gain of CO phase on approaching T_{MI}. The frequency-dependent impedance scales as the function $g(f\xi^{2+\theta})$, with $\theta \approx 0.86$, suggesting anomalous diffusion in percolating clusters.

Thin films of thickness ≈ 200 nm of $La_{0.625-y}Pr_yCa_{0.375}MnO_3$, with $y=0.275$, 0.3, 0.325, 0.35, and

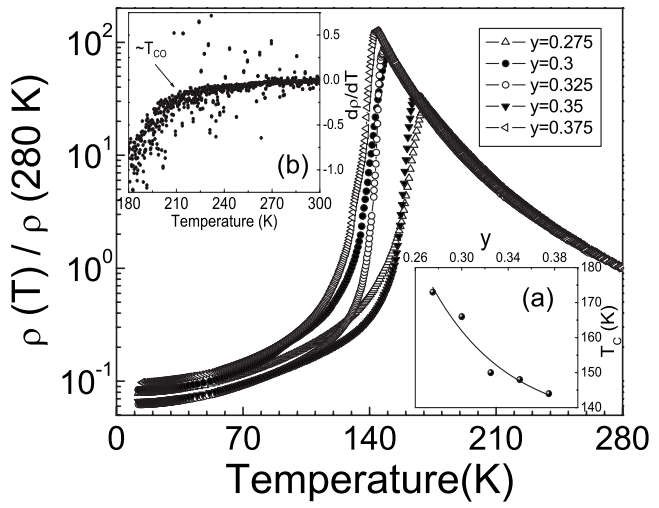

FIG. 1. Temperature dependence of resistivity normalized to its value at 280 K for samples of different y all measured during heating cycle. (b) shows the variation of $\frac{d\rho}{dT}$ with T. The compositional dependence of T_c is shown in (a).

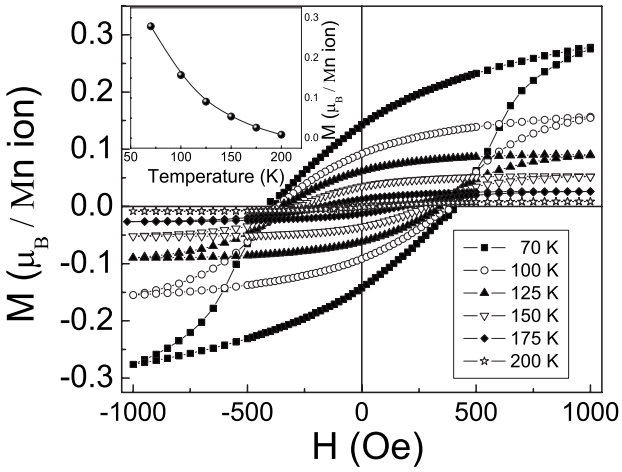

FIG. 2. Magnetization vs field measurements for the $y=0.275$ sample at various temperatures. Inset shows the saturation magnetization as a function of temperature. The absolute value of the magnetic moment is uncertain by ≈50%.

0.375, were grown on (110) oriented single crystals of $NdGaO_3$ (orthorhombic, with $d_{110}=3.8595$ Å) using pulsed laser deposition technique. A KrF excimer laser operated at 10 Hz with an areal energy density of 2 J cm^{-2} per pulse on the surface of a stoichiometric sintered target of LPCMO was used for ablation. The oxygen pressure and the substrate temperature during growth were held at ≈300 mTorr and 750 °C, respectively. Measurements of dc and ac resistivities were carried out on 1 mm wide strips of the film in a four-probe configuration using current source, voltmeter, and HP-4192A impedance analyzer, while magnetization was measured with a superconducting quantum interference device magnetometer. For measurement of dc resistivity, the test current was 10 μA. With the sample resistance of 2 kΩ at ~140 K, the Joule heating is ~0.2 μW. Similarly, for ac measurements, the power dissipation in the samples remains below 100 μW. The *I-V* curves, measured at several temperatures up to a peak current of ~5 mA, remained linear and nonhysteretic, indicating the absence of any heating effects. For magnetic imaging and diffraction, we used the JEM2100F-M, a field emission 200 kV electron microscope with a special custom-made field-free objective lens (residual field <4 Oe). *In situ* cooling and heating experiments were conducted using a Gatan cooling stage filled with liquid helium and/or nitrogen. Transmission electron microscopy (TEM) samples were prepared via standard mechanical thinning and polishing techniques to remove the substrate. The final thinning of the films was done using a Fischione ion miller with a single low voltage argon source at glancing angles and at liquid nitrogen temperature.

The temperature dependence of the resistivity $\rho(T)$, normalized to its value at 280 K, of the sample with $y=0.275$, 0.3, 0.325, 0.35, and 0.375 is shown in Fig. 1. The $\rho(T)$ is marked by a semiconductorlike behavior on cooling below room temperature, followed by an insulator-metal transition at T_{MI} on further cooling, which reveals superheating and supercooling effects, indicating a first-order transition in the system. The critical temperature is also a monotonically decreasing function of y as shown in Fig. 1(a), in agreement with the reported behavior of $La_{0.625-y}Pr_yCa_{0.375}MnO_3$ bulk sample.[11] However, unlike some other CO manganites where a distinct step in the ρ vs T plot at $T>T_{MI}$ marks the onset of charge ordering (T_{CO}), we only see a change in the slope of $\rho(T)$ curve as illustrated in Fig. 1(b). The T_{CO} defined as the onset of a sharp change in the slope of the $\frac{d\rho}{dT}$ vs T curve is ≈210 K, which is in agreement with our TEM results discussed in the later part of this Brief Report.

The magnetization $[M(T,H)]$ signal of these films is overwhelmed by the strong paramagnetic contribution of the

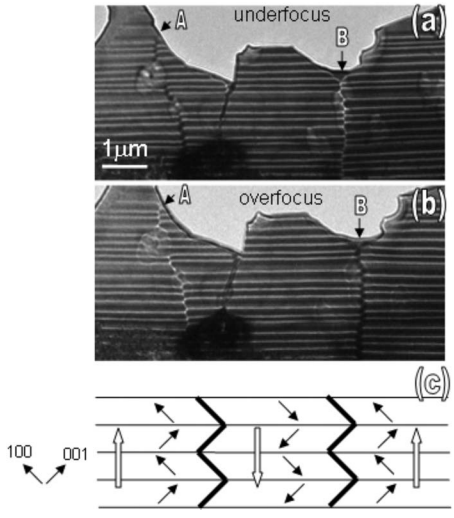

FIG. 3. Lorentz TEM images of $La_{0.625-y}Pr_yCa_{0.375}MnO_3$ ($y=0.275$) at 90 K. (a) Underfocused and (b) overfocused images. (c) Schematic drawing of the local magnetic structure. The image and small arrows represent the magnetization of the primary (180°) and secondary (90°) magnetic domains, respectively. Note that the secondary ferromagnetic domains coincide with the twinning structure of the sample.

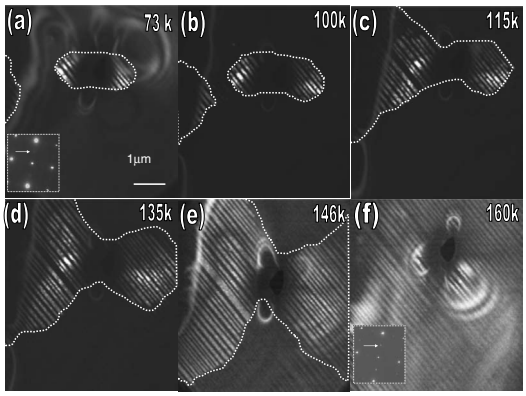

FIG. 4. Dark-field images of $La_{0.625-y}Pr_yCa_{0.375}MnO_3$ ($y=0.275$) recorded using the ($\frac{1}{2}$ 0 2) or (2 0 $\frac{1}{2}$) superlattice reflection showing the evolution and growth of charge-ordered domains at various temperatures: (a) 73 K, (b) 100 K, (c) 115 K, (d) 135 K, (e) 146 K, and (f) 160 K. For clarity, the walls of the charge-ordered domains are outlined. The $(010)^*$ zone diffraction patterns at 73 and 160 K are also included (see insets). Note the significant difference in intensity of the superlattice reflection at the two temperatures.

Nd^{3+} ions of the substrate (NGO), which makes a quantitative measurement of magnetization erroneous by as much as 50%. Nevertheless, the field dependence of magnetization at various temperatures was carefully extracted for the $y=0.275$ sample and is displayed in Fig. 2. The onset temperature of spontaneous magnetization (T_{Curie}) of this sample is $\approx$190 K, which matches with the insulator-metal transition seen in $\rho(T)$ on cooling the sample (Fig. 1). The temperature dependence of saturation moment plotted in the inset of Fig. 2 shows a much steeper rise and a wrong slope at lower temperatures, which is not expected from the spin wave renormalized mean-field dependence of $M(T)$. This observation suggests a percolative growth of the ferromagnetic phase fraction at $T<T_{MI}$. It needs to be pointed out here that in spite of a large error in the measurement of the absolute moment, its value per Mn ion is well below the moment that would result if all Mn^{3+} and Mn^{4+} site spins were aligned ferromagnetically. This observation, which indicates incomplete conversion of the CO phase into the FM phase, is supported unequivocally by our electron microscopy results. The Lorentz TEM images of the sample taken at 90 K and shown in Figs. 3(a) and 3(b) reveal ferromagnetic domains when viewed along the [010] direction in the P_{nma} setting. The horizontal lines in the figure are the twin boundaries associated with the (101) twinning originating from cubic-to-orthorhombic transition at high temperature. In Lorentz-Fresnel mode, black and white contrast of divergent and convergent magnetic domain walls, respectively, can be seen under underfocus and overfocus imaging conditions.[17] There are two sets, primary and secondary, of magnetic domains in the sample. The A and B in Fig. 3 mark a pair of the 180° primary domain walls, with magnetization antiparallel across the walls. The secondary domains are those with the 90° domain walls that coincide with the twin boundaries which are likely to arrest domain motion and result in the large coercive field ($\approx$500 Oe) seen in Fig. 2. Figure 3(c) is a

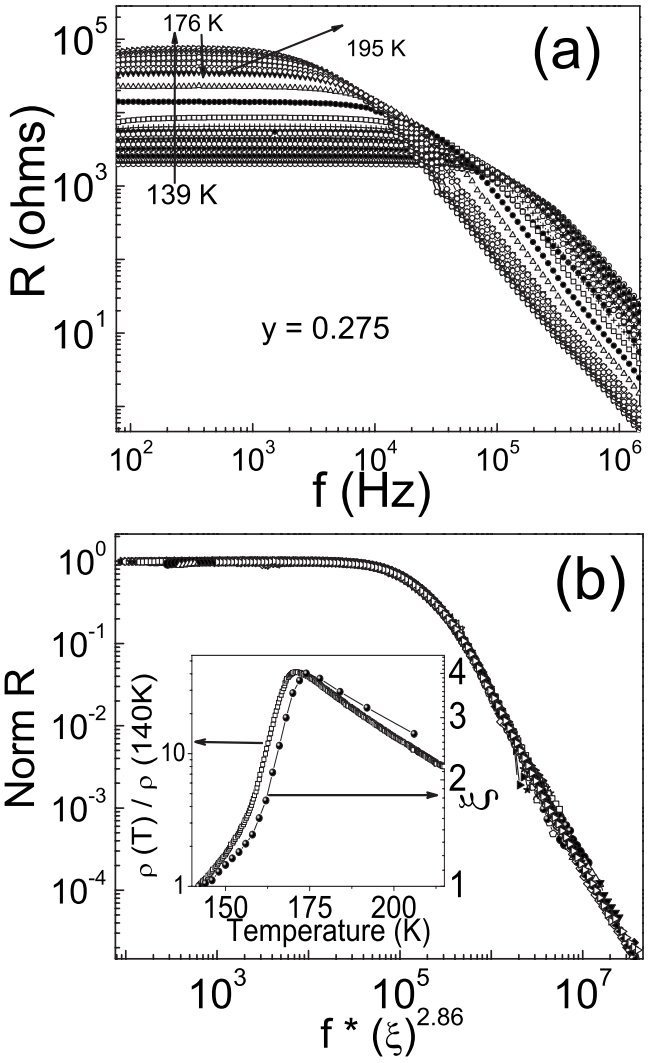

FIG. 5. (a) Frequency dependence of impedance of $y=0.275$ sample at different temperatures. (b) The universal curve generated form the isotherm impedance shown in (a) after scaling. The inset in (b) shows the value of ξ corresponding to different temperatures (right scale). The normalized resistivity is also shown (left scale).

schematic showing the local magnetization. It is important to point out that such FM domains are seen sparsely in the sample, indicating that only a small fraction of the sample volume is ordered ferromagnetically.

To understand the CO and FM phase separation and phase evolution, the samples were imaged at several temperatures between 15 and 300 K in dark field using the ($\frac{1}{2}$ 0 2) or (2 0 $\frac{1}{2}$) superlattice reflection associated with the charge ordering. Figure 4 clearly shows the evolution and growth of CO domains at various temperatures: (a) 73 K, (b) 100 K, (c) 115 K, (d) 135 K, (e) 146 K, and (f) 160 K. Since in this temperature regime twins exist, they are superimposed with CO. The increasing volume fraction of the CO domains is also reflected by the brightness of the superlattice reflections in the $(010)^*$ zone diffraction patterns, as shown in Figs. 4(a) and 4(f). While the limited area of view in dark-field imaging makes it difficult to measure the exact volume fraction of the CO and FM domains as a function of temperature, our esti-

mate yields ≈50% of each phase at ≈70 K, which remains almost constant below 70 K. The sample appears fully charge ordered between 170 and 210 K, and above 210 K, it becomes paramagnetic as indicated by the disappearance of the satellite reflection.

Having established unequivocally a massive PS in the system, we now come to the key issue of ac transport. In Fig. 5(a), we show the frequency (f) dependence of impedance of the $y=0.275$ sample at various temperatures. For $T=139$ K, which is below T_{MI} ($T_{MI}\approx 175$ K for this sample), the FM fraction is large and $p \gg p_c$. The isothermal impedance corresponding to 139 K first remains constant until 10^5 Hz, and then falls off above it as $\approx f^{-x}$ ($x\approx 1.8$). Some of these features of ac conductivity have been seen earlier in related systems.[18,19] As the T_{MI} is approached, the critical frequency (f^*) of deviation from a constant value decreases with temperature for $T<T_{MI}$, and then follows a reverse trend at $T>T_{MI}$. This anomalous behavior of the ac response in the vicinity of T_{MI} is a characteristic feature of percolating systems,[16] which has been explained either by using the ideas of intercluster polarization,[20] in which more of the dangling ends of metallic clusters contribute to conduction at higher frequency, or due to delay time effects on holes whose diffusion length L_f over the fractal network of the PS medium scales as $L_f \sim f^{-1/(\theta+2)}$, where $\theta=(\mu-\beta)/\nu=0.8$ in two-dimensions.[16] Based on the approach of anomalous diffusion, the frequency dependence of the sample impedance has been modeled as,[21]

$$|Z(T,f)| = R(T,0)g(f\xi^{2+\theta}).$$

The different impedance isotherms at $T_{MI}<T<T_{MI}$ with frequency shown in Fig. 5(a) can be fitted to a universal graph shown in Fig. 5(b). This fit was achieved by scaling the frequency as $f\xi^{2+\theta}$ for different temperatures. At each temperature, the value of ξ was chosen to give the best fit to the curve. The correlation length ξ represents the mean spanning length of the ferromagnetic clusters in the critical regime. It is expressed in units of a microscopic length scale b, which could be the size (≈12 Å) of magnetic polarons in these systems as seen in small angle neutron scattering experiments.[22] As shown in the inset, the variation of ξ and resistivity with temperature has the same nature. Similar results were obtained for $y=0.325$ and 0.375 samples.

In summary, we have measured the frequency dependence of impedance of a doped manganite at 3/8 filling ($x=3/8$) in the critical regime of metal-insulator phase transition from CO to FM state. High resolution electron microscopy combined with Lorentz imaging, which established mesoscale phase separation in the material, suggests a percolative character of this MI transition. The scaling behavior of $|Z(T,f)|$ in the critical regime reinforces this conclusion and allows estimation of the mean spanning length of ferromagnetic clusters in the vicinity of T_{MI}.

This work has been supported by internal funding of IIT-Kanpur and the Office of Basic Energy Sciences, U.S. Department of Energy.

*rcb@iitk.ac.in

[1] A. Moreo, S. Yunoki, and E. Dagotto, Science **283**, 2034 (1999).
[2] N. D. Mathur and P. B. Littlewood, Phys. Today **56**, 25 (2003).
[3] M. B. Salamon and M. Jaime, Rev. Mod. Phys. **73**, 583 (2001).
[4] Y. Tokur and Y. Tomioka, J. Magn. Magn. Mater. **200**, 1 (1999).
[5] J. M. D. Coey, M. Viret, and S. von Molnar, Adv. Phys. **48**, 167 (1999).
[6] *Colossal Magnetoresistance, Charge-ordering and Related Aspects of Manganese Oxides*, edited by C. N. R. Rao and B. Raveau (World Scientific, Singapore, 1998).
[7] V. Kiryukhin, B. G. Kim, V. Podzorov, S.-W. Cheong, T. Y. Koo, J. P. Hill, I. Moon, and Y. H. Jeong, Phys. Rev. B **63**, 024420 (2000).
[8] H. J. Lee, K. H. Kim, M. W. Kim, T. W. Noh, B. G. Kim, T. Y. Koo, S.-W. Cheong, Y. J. Wang, and X. Wei, Phys. Rev. B **65**, 115118 (2002).
[9] M. Tokunaga, Y. Tokunaga, and T. Tamegai, Phys. Rev. Lett. **93**, 037203 (2004).
[10] L. Zhang, C. Israel, A. Biswas, R. L. Greene, and A. Lozanne, Science **298**, 805 (2002).
[11] M. Uehara, S. Mori, C. H. Chen, and S.-W. Cheong, Nature (London) **399**, 560 (1999).
[12] J. C. Loudon, N. D. Mathur, and P. A. Midgley, Nature (London) **420**, 797 (2002).
[13] M. Mayr, A. Moreo, J. A. Verges, J. Arispe, A. Feiguin, and E. Dagotto, Phys. Rev. Lett. **86**, 135 (2001).
[14] V. Hardy, A. Wahl, and C. Martin, Phys. Rev. B **64**, 064402 (2001).
[15] R. Zallen, *The Physics of Amorphous Solids* (Wiley, New York, 1983), p. 135.
[16] Y. Gefen, A. Aharony, and S. Alexander, Phys. Rev. Lett. **50**, 77 (1983).
[17] S. J. Lloyd, N. D. Mathur, J. C. Loudon, and P. A. Midgley, Phys. Rev. B **64**, 172407 (2001).
[18] N. K. Pandey, R. P. S. M. Lobo, and R. C. Budhani, Phys. Rev. B **67**, 054413 (2003).
[19] Silvana Mercone, Alexandre Wahl, Alain Pautrat, Michaël Pollet, and Charles Simon, Phys. Rev. B **69**, 174433 (2004).
[20] D. J. Bergman and Y. Imry, Phys. Rev. Lett. **39**, 1222 (1977).
[21] R. B. Laibowitz and Y. Gefen, Phys. Rev. Lett. **53**, 380 (1984).
[22] J. M. De Teresa, M. R. Ibarra, P. A. Algarabel, C. Ritter, C. Marquina, J. Blasco, J. Garca, A. del Moral, and Z. Arnold, Nature (London) **386**, 256 (1997); Ch. Simon, S. Mercone, N. Guiblin, C. Martin, A. Brûlet, and G. André, Phys. Rev. Lett. **89**, 207202 (2002).